Protected gap closing and reopening in topological-insulator Josephson junctions

Jakob Schluck[1,5], Ella Nikodem[1,5], Anton Montag[2,3,4], Alexander Ziesen[2], Mahasweta Bagchi[1], Fabian Hassler[2], Yoichi Ando[1]

[1]*Physics Institute II, University of Cologne, Zülpicher Str. 77, 50937 Köln, Germany*

[2]*Institute for Quantum Information, RWTH Aachen University, 52056 Aachen, Germany*

[3]*Max Planck Institute for the Science of Light, 91058 Erlangen, Germany*

[4]*Department of Physics, Friedrich-Alexander-Universität Erlangen-Nürnberg, 91058 Erlangen, Germany*

[5]*These authors contributed equally*

In the seminal proposal by Fu and Kane, the superconducting proximity effect was predicted to transform the surface state of a topological insulator (TI) into a topological superconductor, forming a nonchiral 1D Majorana state within a linear Josephson junction on the TI surface. The hallmark of this 1D Majorana state is a robust gap closing as a function of the superconducting phase difference φ across the junction, which alternates in and out of the topological phase. These topological phase-transitions occur at $\varphi = (2n + 1)\pi$ with integer n, leading to a 4π-periodicity of the ground state. While the 4π-periodicity has been indirectly inferred in the AC Josephson effect, the direct observation of the 1D Majorana state in a TI Josephson junction has remained contentious. Here, we report the direct observation of topological phase-transitions in a TI Josephson junction, where the local density of states is

1

probed via tunnel contacts and φ is controlled by a flux loop. The observed transitions are independent of the chemical potential, reinforcing their topological origin. Under an applied perpendicular magnetic field, Josephson vortices form, making φ position-dependent. In this case, the gap closing occurs locally at the Josephson vortex cores where $\varphi = (2n + 1)\pi$, which we also observe. Our findings provide direct confirmation of the Fu-Kane proposal and robust evidence for the emergence of topological superconductivity in a TI Josephson junction.

1 Introduction

After more than 100 years from the discovery, superconductors remain a fascinating subject of research in physics. They become even more interesting when topology comes into play[1]. A special type of superconductor, called "spinless chiral p-wave superconductor", is a prototypical topological superconductor hosting Majorana zero-modes at point-defects[1,2]. The Majorana zero-modes obey non-Abelian exchange statistics[3,4], which make them a promising candidate for topological quantum computing[5]. Due to this exciting prospect for applications, the realization of topological superconductivity and the observation of Majorana zero-modes have become major themes in condensed matter physics.

Since a spinless chiral p-wave superconductor is not yet found in nature, there have been significant efforts to effectively realize it in a hybrid system[6,7]. Theoretically, a hybrid of a strongly spin-orbit-coupled material and a conventional superconductor would effectively realize the spinless chiral p-wave pairing due to spin-momentum locking. The earliest of such proposals made by Fu and Kane in 2008 is based on topological insulator (TI) surface states proximitised by a

conventional *s*-wave superconductor[8]. However, even though the spin-momentum locking is most naturally realized in TIs, the experimental evidence for the realization of topological superconductivity obtained so far in this platform is weak and relies on indirect signatures, such as modified Fraunhofer patterns[9–11] and the microwave response[12–14] of a Josephson junction made on a TI, or a broad zero-bias conductance peak (ZBCP) observed in the Abrikosov vortex core of a proximitised TI[15]. The search for Majorana zero-modes has been more advanced on one-dimensional (1D) semiconducting Rashba nanowires, proximity-coupled to a superconductor, and exposed to a strong magnetic field[7]; however, despite a remarkable experimental progress[16,17], the distinction between topological and trivial ZBCPs remains contentious in this 1D platform[18–20]. It has been realized early on[21] and emphasized in the recent literature[22–25] that the direct observation of the topological phase-transition, the closing and reopening of the superconducting (SC) gap, is a more robust signature of a topological superconductor and thus Majorana zero-modes.

In this work, we turn to the TI platform and report the observation of protected gap closing and reopening in a TI Josephson junction upon changing the phase difference φ across the junction, the key signature of the 1D Majorana state predicted by Fu and Kane for a phase-biased TI Josephson junction realizing 1D topological superconductivity[8]. The gap closing and reopening correspond to a switch in the ground-state parity, which implies a change in the $\mathbb{Z}_2$ topological invariant [2] and signals a topological phase-transition of the 1D Majorana state formed in the junction. The phase transition is topologically-protected in the absence of parity-mixing terms. At the phase transition, which occurs at $\varphi = (2n + 1)\pi$ with integer n, the gap closes and a gapless 1D mode appears. Note that the Fu-Kane theory is only valid for a constant φ along the junction.

3

When a perpendicular magnetic field is applied to the junction, rendering φ position-dependent[26], the gapless 1D mode becomes confined at the core of a Josephson vortex, where the local phase difference is $\varphi = (2n + 1)\pi$. Because of this, the gapless 1D mode evolves into a Majorana zero-mode that is bound to the point defect formed by the Josephson vortex. In our experiment, we observe a periodic closing and reopening of the gap by tuning the phase difference across the junction in a SQUID geometry and simultaneously detecting the local density of states (LDOS) at different locations. The gap closing is accompanied by a multitude of low-lying excited states, as expected from theory. We further elucidate the locality of the involved states created by the phase gradient in perpendicular magnetic fields. Our observation is a direct experimental proof of the Fu-Kane theory and is a strong indication of the emergence of topological superconductivity in a TI Josephson junction. Based on this experiment, we discuss the desirable parameter range to realize well-protected Majorana zero-modes in a TI Josephson junction, which turns out to be within experimental reach.

2   Phase-biased topological-insulator Josephon junction

The 1D Majorana state predicted by Fu and Kane has a 4π-periodic φ-dependence at zero momentum as shown in Fig. 1a. The corresponding evolution of the gap in the junction is depicted in Fig. 1c: The gap is trivial for $0 \leq \varphi < \pi$. It closes at the topological phase-transition with $\varphi = \pi$ where the gapless 1D mode (green line) appears, before reopening in the topological regime, with $\pi < \varphi < 3\pi$. In the topological regime the parity of the ground state is odd, meaning that the bound state below the chemical potential μ is filled with an unpaired electron (shown in yellow). Because

of this, the junction returns to the initial state only at $\varphi = 4\pi$. In contrast, for a conventional An-

dreev bound state, a 2π-periodicity is expected, as depicted in Fig. 1b. Here, the dispersion is given

by[27]

$$E = \pm\Delta \sqrt{1 - \tau \sin^2 (\varphi/2)} \, , \tag{1}$$

with τ the transmittance of the state and Δ the induced SC gap in the TI surface directly beneath

the SC electrodes. In such a scenario, the gap can only close for the fine-tuned case of perfect

transmission ($\tau = 1$). Moreover, in this case, the ground-state parity would remain even across the

gap closing as a conventional Andreev bound state is doubly degenerate due to the spin degeneracy.

A scanning electron microscope (SEM) image of our typical device is shown in Fig. 1d.

A Josephson junction is created by a thin film of Al on top of an exfoliated flake of the bulk-

insulating TI material $BiSbTeSe_2$[28, 29]. The two sides of the junction are connected by an Al loop,

which allows us to accurately tune the phase difference φ by applying a perpendicular magnetic

field. Such a device geometry is commonly used to study the bound state spectrum in an SNS-type

Josephson junction via tunnel spectroscopy[30–33]. Normal electrodes made of Au are deposited after

putting a thin layer of Al_2O_3 as a tunnel barrier. Due to the native oxide of Al, its surface can be

treated as an insulator and the overlap to the Au electrodes does not contribute to the transport.

A back-gate voltage can be applied through the degenerately-doped silicon substrate. Therefore,

this setup enables us to directly probe the LDOS of the TI Josephson junction and to test the Fu-

Kane theory[8]. Note that when the perpendicular magnetic field is very weak such that the large

loop is threaded by only a few flux quanta (and no Josephson vortex nucleates in the junction),

the phase φ is almost constant along the junction, a situation akin to the Fu-Kane model. The

5

case at larger magnetic field, when Josephson vortices nucleate in the junction, is discussed later. We focus on the results obtained from a device similar to the one shown in Fig. 1d with two independent tunnel junctions TJ1 and TJ2 located at different positions on the same Josephson junction. Additional data obtained from a second, essentially identical device, is shown in the supplement to demonstrate the reproducibility of our results.

3 Tunnel spectra and protected gap closing

In Fig. 1e, we show the continuous evolution of the differential conductance dI/dV of TJ1 with the applied DC bias voltage V_b and the perpendicular magnetic field B around zero. Line cuts for selected fields are shown in Fig. 1f. Without magnetic field applied, we observe sharp particle-hole symmetric peaks at the bias voltages of $\pm 130\,\mu$eV and a strong reduction in dI/dV at lower bias. The constant dI/dV at higher bias corresponds to a resistance of about $400\,\mathrm{k\Omega}$, indicating we are in the tunnelling regime, where the observed dI/dV is proportional to the LDOS. The peak energy of $130\,\mu$eV is smaller than the SC gap of our Al-film, which can be calculated from the critical temperature to be $170\,\mu$eV. This confirms that the LDOS of the proximitised TI surface, not the LDOS of the Al electrode, is being measured. The LDOS at low bias does not drop to zero but remains finite, which indicates additional in-gap states that are not fully proximitised, consistent with our previous result on similar TI Josephson junctions[34]. Such a soft gap has also been reported for comparable devices based on carbon nanotube[30], graphene[31], HgTe[32], or InAs[33].

As a finite phase bias φ is generated across the junction with the application of a perpendicular magnetic field, the positions of the particle-hole symmetric peaks shift to a lower bias voltage

and their amplitude is diminished. For the magnetic field of about $115\,\mu$T that corresponds to

$\varphi = \pi$, the particle-hole symmetric peaks merge into a single broad peak at zero bias, signalling

the closing of the gap. The spectrum then evolves periodically, with the conductance at $230\,\mu$T

becoming identical to the one observed at zero field. Having the Fu-Kane theory in mind, our

data is consistent with the interpretation that the peak positions trace the gap, corresponding to the

lowest-lying state at zero momentum, that evolves with φ and closes at π (see Fig. 1a). Above

this gap (but still below the bulk gap), there is a continuum of states corresponding to the motion

along the junction[8]. Our LDOS spectra reflects this physics showing a higher conductance above

the gap when compared to the value below. At $\varphi = \pi$, the gap closing indicates a topological

phase-transition[8].

It is important to note that the gap closing is observed despite the moderate interface trans-

parency of our junction. Moderate transparency indicates that the junction transmittance τ is less

than 1, which implies that conventional Andreev bound states should be gapped according to

Eq. (1). Indeed, similar devices made on various materials reported in the literature[30–33] all had

$\tau < 1$ and exhibited gapped spectra at $\varphi = \pi$. In contrast, our observation shows a gap closing,

which is distinctly different from these results in non-topological materials supporting that the gap

closing is of topological origin.

To further corroborate this interpretation, we have performed numerical simulations of the

differential conductance G expected from the 1D Majorana state for the geometry and parameters

of our devices (see supplement for details). Figure 2a shows the calculated G as a function of

7

V_b and φ, while the line cuts for the same φ values as in Fig. 1f are shown in Fig. 2b. These simulations clearly identify the two branches that cross at $\varphi = (2n + 1)\pi$ to be the even- and odd-parity bound states having a 4π-periodicity. In Fig. 2b, the coherence peaks show up at the edge of the excitation gap and they diminish rapidly with increasing φ. Most importantly, the simulations show that the gap closing at $\varphi = \pi$ results in a broad hump rather than a sharp ZBCP. All these results are consistent with our experimental observation.

4 Locality of the gap closing in perpendicular magnetic fields

Next, we study the behaviour of our device in higher magnetic fields and compare the LDOS probed at TJ1 and TJ2. When a perpendicular magnetic field B is applied to the junction, φ becomes dependent on the position along the junction (y direction). If B is strong enough to nucleate Josephson vortices, the position where the local phase difference becomes $\varphi = (2n + 1)\pi$ is identified as the Josephson vortex-core, and the gapless 1D mode in the Fu-Kane theory for global $\varphi = (2n + 1)\pi$ turns into a Majorana zero-mode confined to the Josephson vortex-core[26]. The concept of this Majorana zero-mode generation is sketched in Fig. 3a. A spatially varying phase φ along a TI Josephson junction caused by B leads to a position-dependent gap function $m \propto \cos \frac{\varphi(y)}{2}$ as indicated by the colour code in the junction[26]. Associated with the sign change in the gap function, the gap closes locally at $\varphi(y) = (2n + 1)\pi$ (white area), corresponding to the core of the Josephson vortex, and a Majorana zero-mode (green dots) nucleates that is confined along the junction by the phase gradient. We note that the topologically-protected nature of the gap closing is intuitively understandable in this situation: the region of the junction with $-\pi < \varphi(y) < \pi$ (red)

8

has the even-parity ground state with $\mathbb{Z}_2$ index of 0, whereas the region with $\pi < \varphi(y) < 3\pi$ (blue) has the odd-parity ground state with $\mathbb{Z}_2$ index of 1; therefore, the boundary between the two regions must become gapless for the topological invariant to change.

We indeed observed the locality of this gap closing. The top and bottom panels of Fig. 3c show the dI/dV data simultaneously measured at TJ1 and TJ2 as a function of V_b and B in the 5 – 6 mT range. Both junctions present a comparable evolution of their bound state spectrum, but there is a clear phase shift and their periods are slightly different. For TJ2 we find a periodicity of $200\,\mu$T, smaller than that of TJ1 ($230\,\mu$T). This difference in the period is consistent with the sample geometry (see supplement for details) in which the effective junction area considering the flux focusing effect[34–36] is about ~10% of the loop area. To understand the LDOS at TJ1 and TJ2, we have calculated the expected texture of the gap function based on the device geometry. In our junctions, the self-inductance is negligible and its width is much shorter than the Josephson penetration depth (see supplement), justifying the description of the phase gradient in terms of

$$\varphi(y) = \frac{2\pi B}{\Phi_0}\left(A + yL_{\text{eff}}\right) \ , \tag{2}$$

with A the loop area, $\Phi_0 = \frac{h}{2e}$ the magnetic flux quantum, and L_{eff} the effective length of the junction taking the flux-focusing effect into account. The evolution of the gap function $m \propto \cos\frac{\varphi(y)}{2}$ is calculated from this formula with the loop and junction area as fitting parameters (see supplement) and visualized in the middle panel of Fig. 3c. We show snapshots of the phase-texture in the junction for a range of magnetic fields corresponding to the experimental situation. In this range, there are two to three Josephson vortices inside the junction, whose position is tuned by the global perpendicular magnetic field. They enter the junction from the bottom where TJ2 is located, and

move upwards to TJ1 with increasing magnetic field. Whenever a Josephson vortex-core crosses the location of a tunnel junction, a gap closing is observed. This demonstrates the local nature of the gap closing in the presence of Josephson vortices. The data shown in Fig. 3c was taken at an applied back-gate voltage of $V_G = -5$ V, and we chose the magnetic field range of $5 - 6$ mT for the visibility of the phase gradient. The same pattern was found to continue into higher magnetic fields until the Al superconductivity was suppressed at 15 mT (see supplement).

We note that the spectra shown in Fig. 3c essentially look the same as those in Fig. 1e. This is because the Majorana zero-mode in the Josephson vortex-core is not well-separated in energy. For the conditions realized, it is accompanied by a quasi-continuum of low-energy bound states[26]. Taking the smearing due to the finite-temperature into account, the local spectrum becomes a broad peak, indistinguishable from the Fu-Kane situation. In Fig. 3b, we show the magnitude of the gap function near a Josephson vortex-core and the finite-energy bound states calculated from the model in Ref. 26, along with the spatial extent of the expected Majorana zero-mode. For the parameters relevant to our device with $\mu = 25$ meV, the calculated finite-energy bound states form a quasi-continuum with a minigap of only 2% of Δ (i.e. 3 μeV), which is of the order of the thermal energy at the base temperature.

5 Stability of the gap closing

In the next step, we check the robustness of the observed features with respect to the chemical potential, as tuned by a global back gate. Figure 4a shows the dI/dV data in $B = 0$ T at a high bias voltage ($V_b = 1$ mV) as a function of the back-gate voltage V_G for both TJ1 and TJ2. The

overall tendency is that the conductance decreases for more negative gate-voltages, indicating that the TI surface is in the n-type regime. Superimposed to this general trend, we observe broad peaks (typical peak width of a few V), which are commonly found in dielectric-based tunnelling devices and conventionally explained by resonant states in the dielectric[31]. Figure 4b presents the V_G-dependencies of the normalized conductance spectra obtained at TJ1: the upper and lower panels show the evolutions of the maximum excitation gap for $\varphi = 0$ (upper) and the spectrum observed for $\varphi = \pi$ (lower) in a wide range of V_G from -20 to $+20$ V. The maximum excitation gap is very stable, indicating that the resonance states due to impurities are not affecting the proximity-induced gap. On the other hand, the position of the conductance peak for $\varphi = \pi$ is slightly shifted to the negative V_b side at $V_G \approx 12 - 20$ V, which is probably due to an influence of the strong resonance states located around 13 V (see Fig. 4a). Remarkably, the broad ZBCP that accompanies the gap closing is stable for a wide range of V_G from -10 V to $+12$ V. It is worth noting that the ZBCP observed in this V_G range is not correlated with the weaker resonance states seen in Fig. 4a, which further supports the intrinsic origin of the gap closing. For $V_G \lesssim -10$ V, the gap closing is not accompanied by a clear ZBCP. We believe that this is because our non-tunable tunnel contacts did not couple sufficiently well to the bound states in this regime, preventing us from resolving a peak.

In Figs. 4c and 4d, we show the B-dependencies of the normalized conductance spectra for equally-spaced V_G values between -20 and $+20$ V for both TJ1 and TJ2. One can immediately see that the basic magnetic-field-periodic change in dI/dV is very stable at all V_G values. However, upon close inspection, the occasional breaking of exact electron-hole symmetry is visible. Particularly in TJ1, the tunnel-coupling of the electrode to the electron and hole states in the TI

11

surface is modified by back gating: At $V_G = -10\,\text{V}$, the electron-like bound states give a stronger signal than the hole-like ones, whereas the situation is reversed for $V_G = +15\,\text{V}$. Similar behaviour has been reported for comparable devices, e.g., based on carbon nanotubes[30], and it was explained to be due to state-dependent tunnel couplings. Overall, we conclude that the gap closing is robust with respect to changes of the chemical potential indicating that we observe a topological phase-transition.

In passing, we mention that in a device where the tunnel barrier was not in a favourable condition to probe the TI surface, we observed strongly dispersing bound states in a very narrow range of V_G associated with a spurious ZBCP occurring at a particular V_G value (see supplement). These features are consistent with the Andreev quantum-dot states predicted in Ref. 37, which might occur in the dielectric. The observations of two different types of ZBCPs, stable and spurious, give confidence that the former is associated with an intrinsic gap closing.

6 Discussions

Our observation of a stable gap closing and reopening in a TI Josephson junction having only a moderate transparency cannot be understood in terms of conventional Andreev bound states and gives the first direct proof of the topological phase-transition predicted by the Fu-Kane theory. To firm up the appearance of topological superconductivity, it would be an interesting future experiment to employ a charge sensing technique[38] in order to detect the parity change in the junction before and after the gap closing. Of course, the definitive proof of topological superconductivity is the observation of Majorana zero-modes, well-protected by a substantial excitation gap, and

the demonstration of their non-Abelian exchange statistics through braiding. In a TI Josephson junction, well-protected Majorana zero-modes can in principle be generated in Josephson vortex-cores as we discuss below. Once such protected Majorana zero-modes are generated, they can be physically moved along the junction in a controlled manner[39]; this degree of freedom allows us to conceive braiding operations in a three-slit Josephson junction[39] and the resulting change in the parity can be detected by charge sensing[38]. Another possibility to confirm the non-Abelian statistics is to build a Josephson-vortex interferometer proposed by Grosfeld and Stern[40], which detects the result of braiding using the Aharonov-Casher effect.

Let us estimate the necessary parameter range to obtain well-protected Majorana zero-modes in Josephson vortex-cores. There are two quantities that are crucial for this consideration: One is the spatial extent of the Majorana zero-mode $\lambda_B = \sqrt{v_M l_B / \pi \Delta}$, where $l_B = \Phi_0 / (B L_{\text{eff}})$ is the distance between Josephson vortices in the junction and v_M is the renormalized Majorana velocity. To calculate v_M, we use the formula (see supplement for details)

$$v_M = v_F \left(\frac{\Delta^2}{\Delta^2 + \mu^2} \right) \frac{\cos\left(\frac{\mu L}{\hbar v_F}\right) + \frac{\Delta}{\mu} \sin\left(\frac{\mu L}{\hbar v_F}\right)}{1 + \frac{\Delta L}{\hbar v_F}} \tag{3}$$

valid in the short-junction regime $L \lesssim \hbar v_F / \Delta$ (L is the true length of the junction). For large $\mu \gg \Delta$, the formula goes over to the simple expression $v_M \simeq v_F (\Delta/\mu)^2$ given in Ref. 26. The other important quantity is the energy of the first excited state, which is given as $E_1 \approx \sqrt{2\pi v_M \Delta / l_B}$ near $\varphi = (2n + 1)\pi$ [26]. Note that reducing μ enhances v_M, and thus E_1 and λ_B. However, λ_B must be shorter than $l_B/2$ to avoid the overlap of neighbouring Majorana zero-modes which bounds μ from below. To see this competition, we theoretically consider the case of using Nb for the SC electrodes. We calculate the dependencies of λ_B and E_1 on μ and B. The results, shown in Figs. 2c

and 2d, indicate that a moderately large μ is indeed helpful to realize a short λ_B and the magnetic field helps to obtain a usefully large E_1. In Fig. 2d, we draw the boundaries to guarantee a sufficient separation of Majorana zero-modes ($\lambda_B/l_B < 0.2$, blue line) and a sufficiently large excitation gap ($E_1/\Delta > 0.2$, green line). In the region between the blue and green lines, see Fig. 2d, Majorana zero-modes are well-protected. In fact, these estimates suggest that it is not necessary to tune μ very close to the Dirac point as long as a magnetic field of the order of 100 mT is used to generate Josephson vortices — an encouraging result for the prospects of Majorana zero-modes in this platform. It is prudent to note that the soft gap, which we observed in our devices, is a problem for braiding, and a hard gap must be realized by improving the interface transparency between the TI and a superconductor. In this regard, we envision the use of the self-epitaxy technique discovered for proximitising $(Bi_{1-x}Sb_x)_2Te_3$ thin films with the $PdTe_2$ superconductor, because a very high transparency of 0.96 was achieved with this technique[41].

In conclusion, we have observed periodic gap-closing and reopening in a phase-biased TI Josephson junction via tunnelling spectroscopy. We have shown that this phenomenon is robust as a function of an extended parameter range in the chemical potential and the perpendicular magnetic field. The robustness of the observed gap closing and reopening is in sharp contrast to the signal expected for a conventional moderate-transparency Josephson junction or other types of zero-energy states which originate from Andreev quantum-dot states[37]. The robustness of the gap closing and reopening is a key feature of the topological phase-transition that occurs in the 1D Majorana state as a function of φ. In the magnetic-field range where a couple of Josephson vortices nucleate in the junction, we have observed the locality of the gap closing implying a con-

finement of the zero-energy mode[26]. However, within the magnetic-field range where Al remains superconducting, an abundance of low-lying excited states arises and this leads to spectra that are indistinguishable from the gap closing of an extended 1D Majorana mode. We have discussed the necessary parameter range to realize well-protected Majorana zero-modes in the Josephson vortex core. Intriguingly, we found that maintaining a chemical potential μ not too close to the Dirac point is crucial to avoid Majorana delocalisation; a μ of approximately 25 meV facilitates the realization of well-protected Majorana zero-modes in a magnetic field of 100 mT accessible with a Nb electrode. Considering the high controllability of the Josephson vortex, this result is promising for braiding experiments. Overall, our experiment elucidates the topological nature of a TI Josephson junction and underscores the realistic prospect of generating well-protected Majorana zero-modes in this system.

Methods

Materials and device fabrications: Bulk single crystals of $BiSbTeSe_2$ were synthesized by the modified Bridgman method using high-purity (99.9999%) Bi, Sb, Te, and Se as starting materials by following the recipe described in Ref. 28. We mechanically exfoliated ultra-thin $BiSbTeSe_2$ flakes from bulk single crystals on degenerately-doped Si wafers covered by 280 nm SiO_2. The latter acts as dielectric for the back gate. $BiSbTeSe_2$ flakes suitable for device fabrication were identified under an optical microscope. The junctions were defined by electron beam lithography. PMMA A4 resist was exposed using a Raith PIONEER Two system. After development, residual resist in the contact areas was removed by a gentle oxygen plasma treatment. Subsequent cleaning in a hydrochloric acid solution shortly before metallisation ensured the removal of any oxide layer.

Then, 3 nm + 45 nm Ti/Al contacts were thermally evaporated after a gentle in-situ Ar cleaning and the device was exposed to air to form a native Al_2O_3 layer. An additional atomic layer deposition of a thin Al_2O_3 layer onto the whole device was performed at 80 °C using Ultratec Savannah S200 to form a tunnel barrier. For the fabrication of the tunnel electrodes, another electron beam lithography was performed to define the pattern. A 5-nm-thick Pt layer was sputter-deposited to act as wetting layer, followed by sputtering an additional 45-nm-thick Au layer. The contact resistances achieved by this procedure are typically larger than 100kΩ, ensuring electron tunnelling to be the prevalent form of transport. The precise device geometry was determined by scanning electron microscopy after the measurements were finished.

Measurements: Transport measurements were performed at base temperature (~50 mK) of our dry dilution refrigerator (Oxford Instruments TRITON 300). Electrical lines incorporate RC and copper-powder filters to reduce noise. Using a two-probe configuration, the differential conductance dI/dV was measured between each individual tunnel electrode and the SC electrode with a standard low-frequency lock-in technique using a Basel instruments current preamplifier. A small DC-offset introduced by the preamplifier was numerically corrected for after the measurements. An AC voltage of 5–10 μV was superimposed to a DC bias voltage. For investigations of the magnetic field dependence, we used our integrated 6/1/1-T superconducting vector magnet.

Simulations: To qualitatively reproduce the conductance spectrum of the TI Josephson junction, a transport simulation was performed using the Python library Kwant[42]. As a model for the three-dimensional strong TI, the Bernevig-Hughes-Zhang model was chosen and implemented on a cubic lattice. Superconductivity was included in the Bogoliubov–de-Gennes formalism. The system has

been extended infinitely along the junction and probed by a tunnel lead attached perpendicularly to the junction. For more information see supplement.

Author contributions: MB grew the BSTS2 crystals, JS and ENN fabricated the devices, performed the experiments and analysed the data together with YA. AM and AZ performed numerical calculations, FH and YA conceived and supervised the project. JS, FH, and YA wrote the manuscript with input from all authors.

Competing Interests: The authors declare no competing interests.

Correspondence: Correspondence and requests for materials should be addressed to Y.A. (ando@ph2.uni-koeln.de).

Data availability: The data that support the findings of this study are available at the online depository zenodo with the identifier 10.5281/zenodo.11615514 and in Supplementary Information.

References

1. Sato, M. & Ando, Y. Topological superconductors: a review. Rep. Prog. Phys. **80**, 076501 (2017).

2. Kitaev, A. Y. Unpaired Majorana fermions in quantum wires. Physics-Uspekhi **44**, 131 (2001).

3. Read, N. & Green, D. Paired states of fermions in two dimensions with breaking of parity and time-reversal symmetries and the fractional quantum hall effect. Phys. Rev. B **61**, 10267–10297 (2000).

4. Ivanov, D. A. Non-abelian statistics of half-quantum vortices in p-wave superconductors. Phys. Rev. Lett. **86**, 268–271 (2001).

5. Nayak, C., Simon, S. H., Stern, A., Freedman, M. & Das Sarma, S. Non-abelian anyons and topological quantum computation. Rev. Mod. Phys. **80**, 1083–1159 (2008).

6. Alicea, J. New directions in the pursuit of Majorana fermions in solid state systems. Rep. Prog. Phys. **75**, 076501 (2012).

7. Flensberg, K., von Oppen, F. & Stern, A. Engineered platforms for topological superconductivity and Majorana zero modes. Nat. Rev. Mater. **6**, 944–958 (2021).

8. Fu, L. & Kane, C. L. Superconducting proximity effect and Majorana fermions at the surface of a topological insulator. Phys. Rev. Lett. **100**, 096407 (2008).

9. Williams, J. R. et al. Unconventional josephson effect in hybrid superconductor-topological insulator devices. Phys. Rev. Lett. **109**, 056803 (2012).

10. Kurter, C., Finck, A. D. K., Hor, Y. S. & van Harlingen, D. J. Evidence for an anomalous current–phase relation in topological insulator Josephson junctions. Nat. Commun. **6** (2013).

11. Yue, G. et al. Signatures of Majorana bound states in the diffraction patterns of extended superconductor–topological insulator–superconductor josephson junctions. Phys. Rev. B **109**, 094511 (2024).

12. Wiedenmann, J. et al. 4π-periodic Josephson supercurrent in HgTe-based topological Josephson junctions. Nat. Communun. **7**, 10303 (2016).

13. Deacon, R. S. et al. Josephson radiation from gapless Andreev bound states in HgTe-based topological junctions. Phys. Rev. X **7**, 021011 (2017).

14. Schüffelgen, P. et al. Selective area growth and stencil lithography for in situ fabricated quantum devices. Nat. Nanotechnol. **14**, 825–831 (2019).

15. Xu, J.-P. et al. Experimental detection of a Majorana mode in the core of a magnetic vortex inside a topological insulator-superconductor Bi_2Te_3/$NbSe_2$ heterostructure. Phys. Rev. Lett. **114**, 017001 (2015).

16. Krogstrup, P. et al. Epitaxy of semiconductor-superconductor nanowires. Nat. Mater. **14 4**, 400–6 (2014).

17. Aghaee, M. et al. InAs-Al hybrid devices passing the topological gap protocol. Phys. Rev. B **107**, 245423 (2023).

18. Valentini, M. et al. Nontopological zero-bias peaks in full-shell nanowires induced by flux-tunable Andreev states. Science **373**, 82–88 (2021).

19. Das Sarma, S. In search of Majorana. Nat. Phys. **19**, 165–170 (2023).

20. Hess, R., Legg, H. F., Loss, D. & Klinovaja, J. Trivial Andreev band mimicking topological bulk gap reopening in the nonlocal conductance of long rashba nanowires. Phys. Rev. Lett. **130**, 207001 (2023).

21. Akhmerov, A. R., Dahlhaus, J. P., Hassler, F., Wimmer, M. & Beenakker, C. W. J. Quantized conductance at the majorana phase transition in a disordered superconducting wire. Phys. Rev. Lett. **106**, 057001 (2011).

22. Rosdahl, T. O., Vuik, A., Kjaergaard, M. & Akhmerov, A. R. Andreev rectifier: A nonlocal conductance signature of topological phase transitions. Phys. Rev. B **97**, 045421 (2018).

23. Pikulin, D. I. et al. Protocol to identify a topological superconducting phase in a three-terminal device (2021). `2103.12217`.

24. Banerjee, A. et al. Local and nonlocal transport spectroscopy in planar Josephson junctions. Phys. Rev. Lett. **130**, 096202 (2023).

25. Banerjee, A. et al. Signatures of a topological phase transition in a planar Josephson junction. Phys. Rev. B **107**, 245304 (2023).

26. Potter, A. C. & Fu, L. Anomalous supercurrent from Majorana states in topological insulator josephson junctions. Phys. Rev. B **88**, 121109 (2013).

27. Beenakker, C. W. J. Universal limit of critical-current fluctuations in mesoscopic Josephson junctions. Phys. Rev. Lett. **67**, 3836 (1991).

28. Ren, Z., Taskin, A. A., Sasaki, S., Segawa, K. & Ando, Y. Optimizing $Bi_{2-x}Sb_xTe_{3-y}Se_y$ solid solutions to approach the intrinsic topological insulator regime. Phys. Rev. B **84**, 165311 (2011).

29. Arakane, T. et al. Tunable Dirac cone in the topological insulator $Bi_{2-x}Sb_xTe_{3-y}Se_y$. Nat. Commun. **3**, 636 (2012).

30. Pillet, J.-D. et al. Andreev bound states in supercurrent-carrying carbon nanotubes revealed. Nat. Phys. **6**, 965–969 (2010).

31. Bretheau, L. et al. Tunnelling spectroscopy of Andreev states in graphene. Nat. Phys. **13**, 756+ (2017).

32. Ren, H. et al. Topological superconductivity in a phase-controlled Josephson junction. Nature **569**, 93 – 98 (2018).

33. Fornieri, A. et al. Evidence of topological superconductivity in planar Josephson junctions. Nature **569**, 89 – 92 (2018).

34. Ghatak, S. et al. Anomalous Fraunhofer patterns in gated Josephson junctions based on the bulk-insulating topological insulator $BiSbTeSe_2$. Nano Lett. **18**, 5124–5131 (2018).

35. Moehle, C. M. et al. Controlling Andreev bound states with the magnetic vector potential. Nano Lett. **22**, 8601–8607 (2022).

36. Banerjee, A. et al. Control of Andreev bound states using superconducting phase texture. Phys. Rev. Lett. **130**, 116203 (2023).

37. Oriekhov, D. O., Cheipesh, Y. & Beenakker, C. W. J. Voltage staircase in a current-biased quantum-dot Josephson junction. Phys. Rev. B **103**, 094518 (2021).

38. Ben-Shach, G. et al. Detecting Majorana modes in one-dimensional wires by charge sensing. Phys. Rev. B **91**, 045403 (2015).

39. Hegde, S. S. et al. A topological Josephson junction platform for creating, manipulating, and braiding Majorana bound states. Ann. Phy. **423**, 168326 (2020).

40. Grosfeld, E. & Stern, A. Observing Majorana bound states of josephson vortices in topological superconductors. Proc. Natl. Acad. Sci. **108**, 11810–11814 (2011).

41. Bai, M. et al. Novel self-epitaxy for inducing superconductivity in the topological insulator $(Bi_{1-x}Sb_x)_2Te_3$. Phys. Rev. Mater. **4**, 094801 (2020).

42. Groth, C. W., Wimmer, M., Akhmerov, A. R. & Waintal, X. Kwant: a software package for quantum transport. New J. Phys. **16**, 063065 (2014).
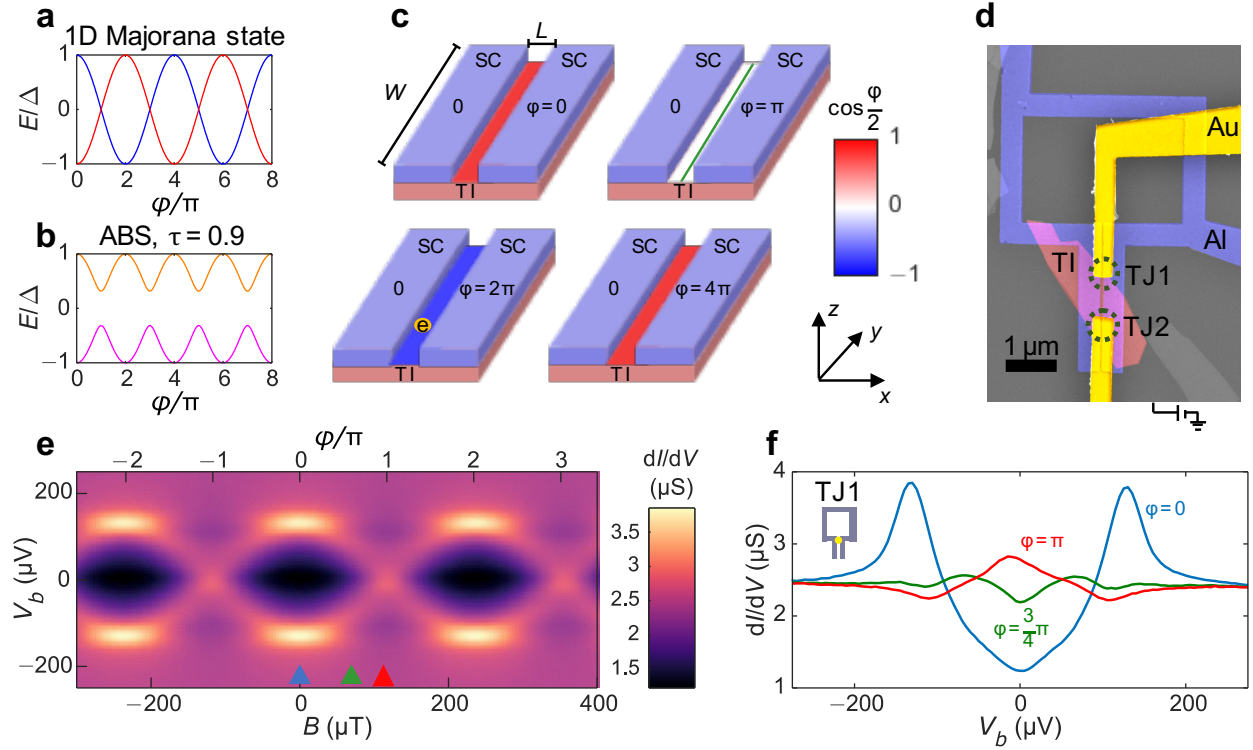
Figure 1: **Device schematics and characterization. a,b,** Comparison of the characteristic phase-dispersions of a 1D Majorana state (**a**) and conventional Andreev bound state (ABS) with transmission coefficient $\tau = 0.9$ (**b**). In panel **a**, the red and blue lines correspond to the even- and odd-parity bound states, respectively. **c,** Evolution of the topological phase in the junction; here, the junction area is coloured according to the gap function $m \propto \cos\frac{\varphi(y)}{2}$ (see the colour scale). As the phase difference across the TI Josephson junction is tuned, the nature of the gap changes from trivial ($\varphi = 0$, red) to topological ($\varphi = 2\pi$, blue). This is accompanied by a change in ground state parity from even to odd, as indicated by the extra electron (yellow) in the junction. In-between, the gap has to close ($\varphi = \pi$) via a gapless Majorana mode (green line). As the phase difference reaches $\varphi = 4\pi$, a full period is completed. **d,** False-colour SEM image of a typical device. The exfoliated TI flake is highlighted in red. The superconductor (blue) is made in a loop geometry to allow for fine-tuning of φ. Metallic contacts (Au) allow for probing the phase-dependent LDOS at two positions (TJ1 and TJ2) in the junction. **e,** Colour mapping of dI/dV in the B vs V_b plane measured on TJ1 at 50 mK with $V_G = 0$ V. At $\varphi = 0$ (mod 2π), a proximity-induced gap opens with conductance peaks at $\pm 130\,\mu$V. The gap closes and a broad ZBCP is observed at $\varphi = \pi$. A periodicity of $230\,\mu$T is observed, consistent with the device geometry. **f,** Line-cuts of the data in **e** at three selected magnetic fields corresponding to $\varphi = 0$, $\frac{3}{4}\pi$, and π.
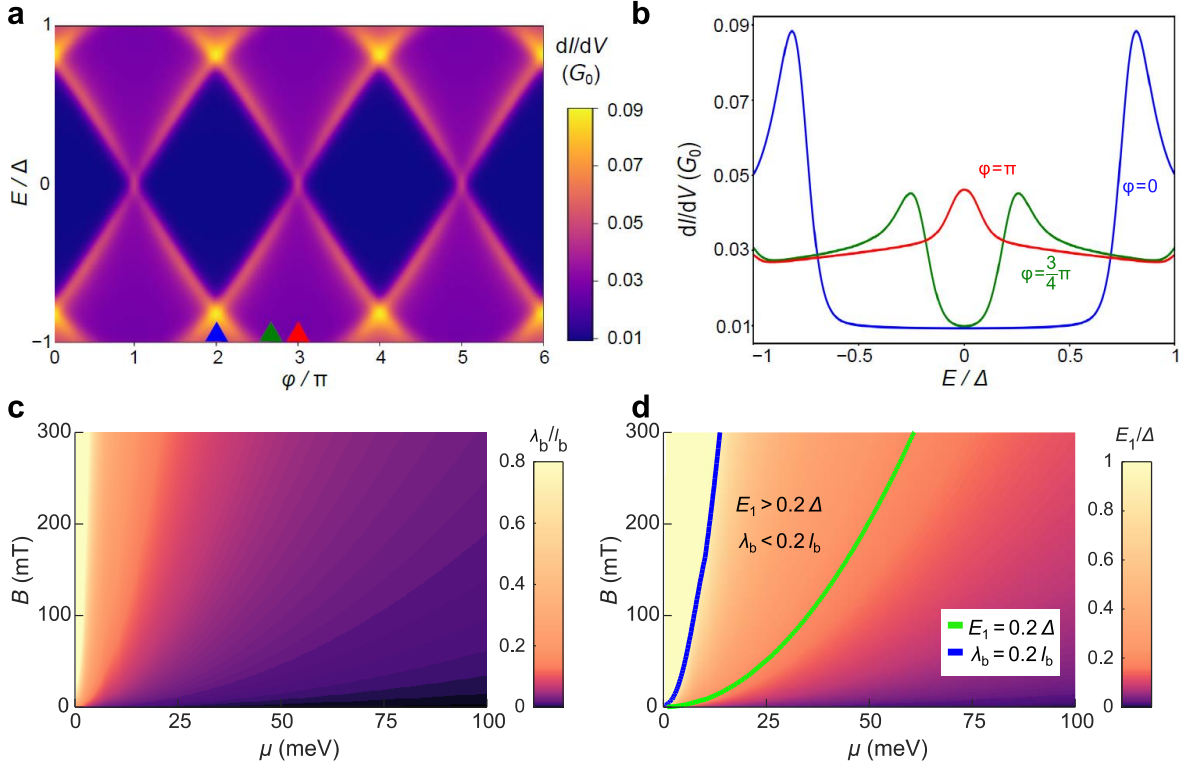
Figure 2: **Theoretical simulations. a,** Colour-mapping of the simulated differential conductance G in units of the conductance quantum $G_0 = e^2/h$ due to the 1D Majorana state as a function of V_b and φ for a temperature $T = \Delta/(30k_B)$ in the Fu-Kane regime with φ constant along the junction. The simulations agree with the experimental observations that the gap (dark region) is periodically modulated and a topological gap closing at $\varphi = \pi$ is observed. **b,** Simulated behaviour of the differential conductance $G(V_b)$ at $\varphi = 0$, $\frac{3}{4}\pi$, and π, which correspond to those shown in Fig. 1f. Note that in the simulation only the surface states and a single transversal mode are taken into account which explains the softer-gap in the experimental results of Fig. 1. **c,d** Calculated dependencies of the Majorana bound state width λ_B and the first excited state energy E_1 on the chemical potential μ and the perpendicular magnetic field B for the Majorana zero-mode generated at the Josephson vortex-core. We used $L = 50$ nm, $v_F = 5.5 \times 10^5$ m/s, and $\Delta = 1$ meV assuming an improved setup with Nb as the SC. The blue and green lines in panel **d** are the boundaries to guarantee a sufficient separation of Majorana zero-modes ($\lambda_B/l_B < 0.2$ obtained from panel **c**) and a sufficiently large excitation gap ($E_1/\Delta > 0.2$), respectively. Majorana zero-modes are well-protected in the relatively broad region between the blue and green lines.
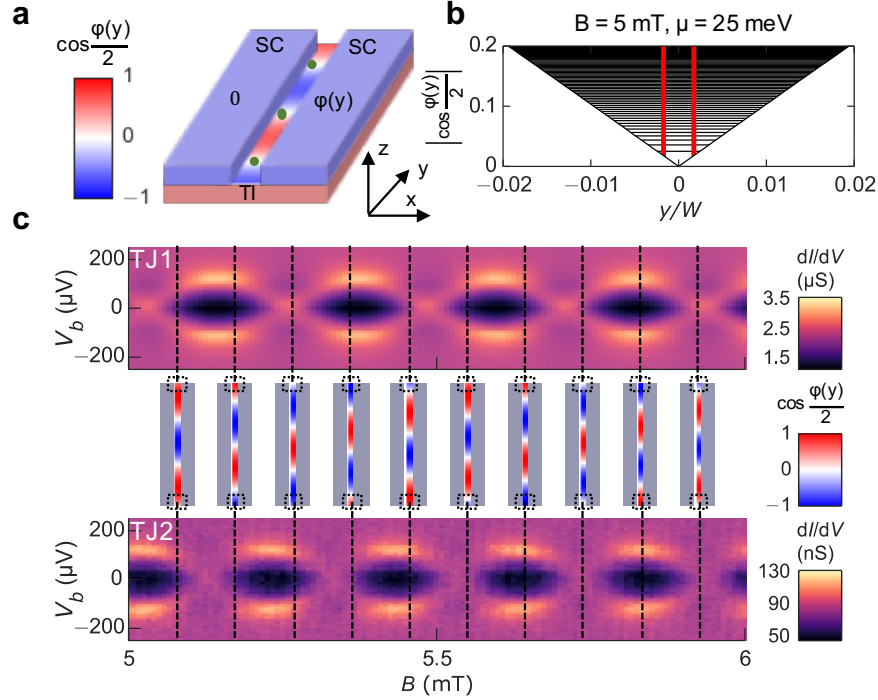
Figure 3: **Locality of the gap closing.** **a,** Schematic drawing of a planar TI Josephson junction in a perpendicular magnetic field, which generates a position-dependent phase $\varphi(y)$ across the junction. The distribution of the topological gap function $m \propto \cos\frac{\varphi(y)}{2}$ is depicted in the junction with a colour scale. The position of $\varphi(y) = (2n + 1)\pi$ corresponds to the Josephson vortex-core, where the gap closes (white colour) and a Majorana zero-mode (green dot) appears. **b,** Position-dependent gap $|m| = |\cos\frac{\varphi(y)}{2}|$ near a Josephson vortex-core in a magnetic field of $B = 5$ mT, plotted with the excited states calculated from the model of Ref. 26 for a chemical potential $\mu = 25$ meV and $\Delta = 0.17$ meV (thin horizontal lines), which form a quasi-continuum with a minigap of only 2% of Δ. The vertical red lines mark the spatial extent of the expected Majorana zero-mode appearing around $y = 0$. **c,** Colour mapping of dI/dV in the B vs V_b plane for TJ1 (top panel) and TJ2 (bottom panel) measured in the magnetic field range of $5 - 6$ mT at 50 mK with $V_G = -5$ V. Note the slight difference in the periodicity, which is 230 μT for TJ1 and 200 μT for TJ2. The middle panel depicts how the distribution of the topological gap function in the junction calculated with Eq. (2) evolves with magnetic fields; the position where the gap function locally becomes zero with $\varphi(y) = (2n + 1)\pi$ corresponds to local gap closing (white regions).
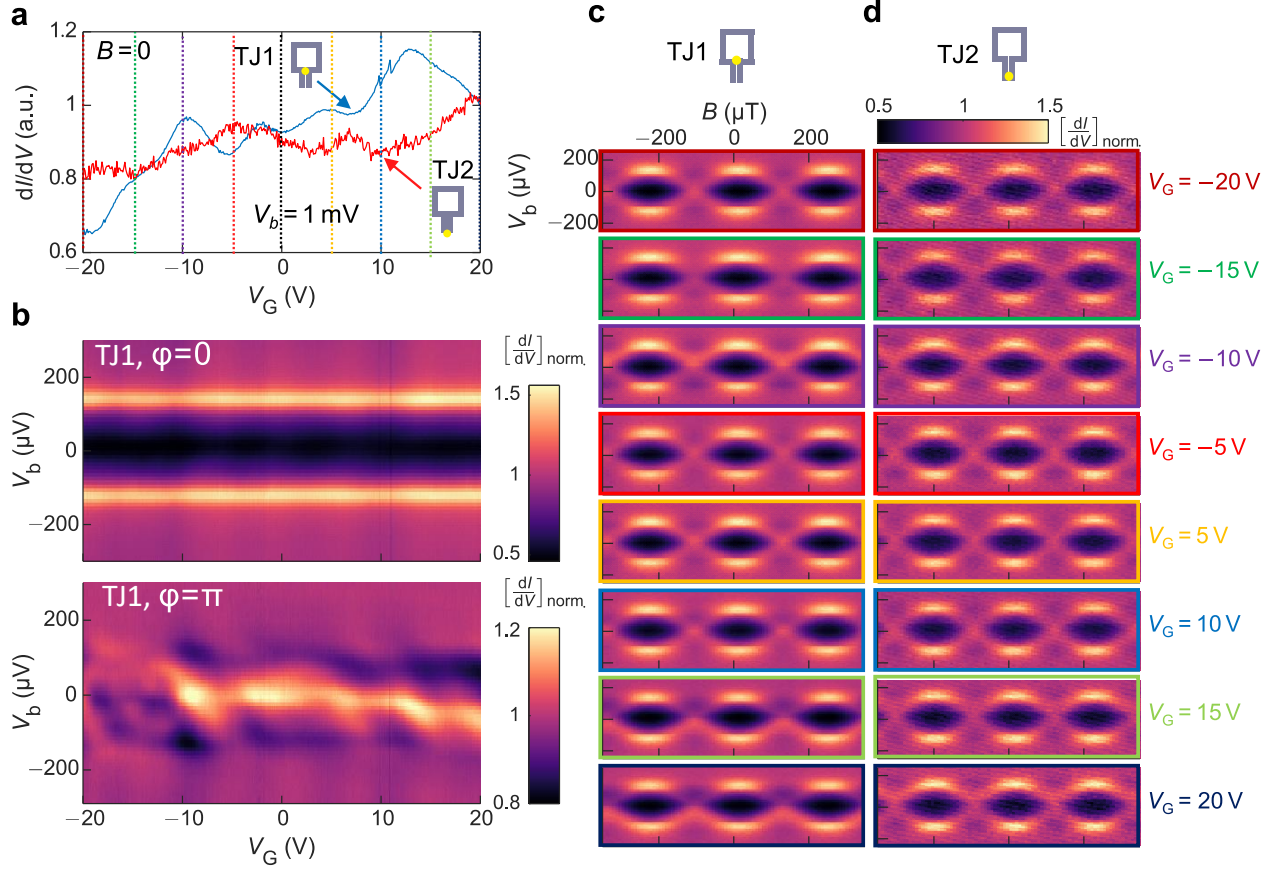
25

Figure 4: **Stability of the gap closing and reopening against a change in the chemical potential. a,** Differential conductance at a high bias voltage of 1 mV as a function of globally-applied back-gate voltage V_G. For both tunnel contacts TJ1 and TJ2, the overall conductance is reduced for more negative gate voltages, indicating an n-type regime. The vertical dashed lines denote the gate voltages for which the continuous evolution of the spectrum is shown in panels **c** and **d**. **b,** Normalized dI/dV, denoted $\left[\frac{dI}{dV}\right]_{norm}$, for TJ1 mapped in the V_b vs V_G plane for $\varphi = 0$ (upper panel) and $\varphi = \pi$ (lower panel). The normalization was done at each V_G by using the dI/dV value at $V_b = 0.3$ mV as reference. **c,d,** Evolution of the B-dependence of the spectrum for a wide range of V_G from -20 to $+20$ V for TJ1 (**c**) and TJ2 (**d**). The V_G values selected for the presentation are equally spaced.

Supplementary information for "Protected gap closing and reopening in topological insulator Josephson junctions"

Supplementary Note 1   Sample geometry and flux focusing

The inner area of the loop is given by $W_L \times H_L = 2.15 \times 3\ \mu\mathrm{m}^2$, while the junction has a width of 3 μm and a length of about 50 nm. The superconducting (SC) electrodes have a width of 400 nm. Making a simple assumption that the flux expulsion from the SC electrodes leads to an increase of the magnetic fluxes for which half the electrode width should be taken into accout, we obtain an expected periodicity of $\Delta B_1 = 196\ \mu$T for TJ1 and $\Delta B_2 = 225\ \mu$T for TJ2, in excellent agreement with our experimental data.

Supplementary Note 2   Data in higher magnetic fields

In Fig. S1, we show the dI/dV spectra on TJ1 and TJ2 from 0 T to 15 mT, which was the maximum available magnetic field in this experiment due to the limitation of the high-resolution current source (Keithley 2450) used for energizing the superconducting magnet in the very low magnetic-field range. The superconductivity in the Al electrode was strongly suppressed in 15 mT, which can be seen in the suppression of the induced gap. Nevertheless, the gap closing and reopening continues in the whole magnetic-field range. For our Al films of thickness 45 nm, we typically observe a critical field of $\sim$20 mT.
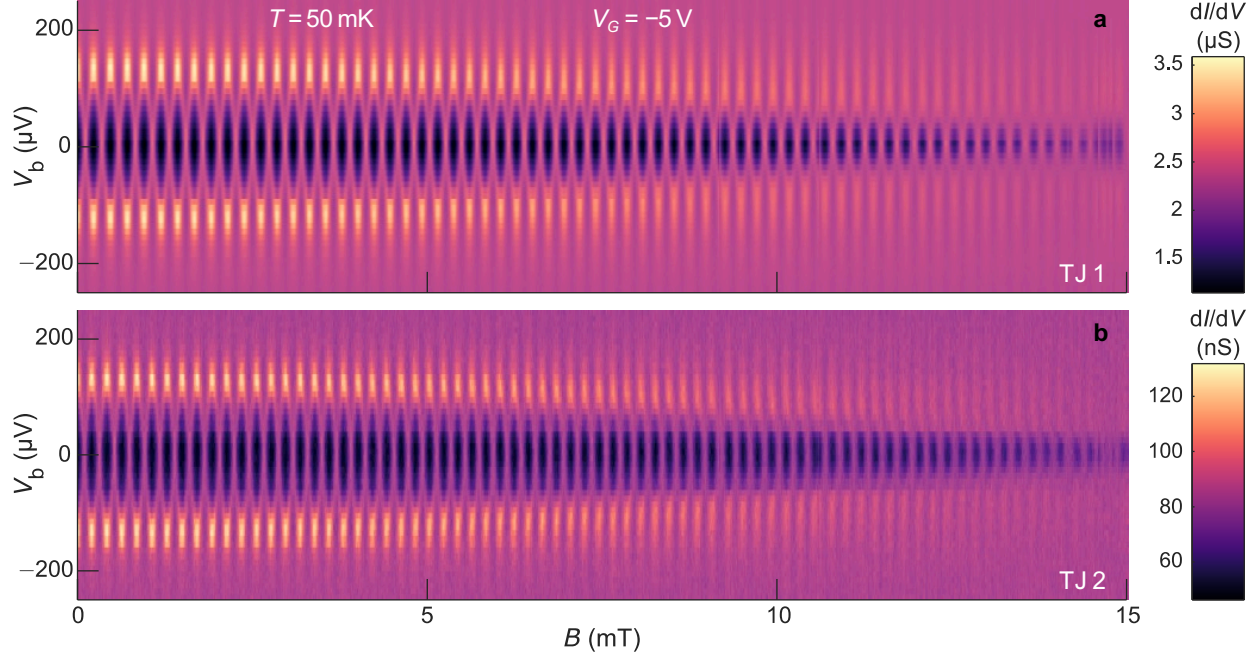
Figure S1: dI/dV spectra measured at TJ1 and TJ2 of the device discussed in the main text for the full magetic field range that was available in this experiment. A gradual reduction of the induced gap is observed in both junctions.

Supplementary Note 3 Josephson penetration length

The RF-SQUID geometry of our device does not allow for a direct measurement of its critical current. However, in comparable devices [1], we typically find a critical current per unit width of the Josephson junction $I_c/W \approx 100\,\mathrm{nA}/\mu\mathrm{m}$. We use this value to estimate the Josephson penetration length in our device using $\lambda_J = \sqrt{\frac{\Phi_0 W^2 t}{4\pi \mu_0 I_c \lambda^2}}$, where $W = 3\,\mu\mathrm{m}$ is the width of the junction, $t = 2\,\mathrm{nm}$ is the extension of the surface state[2], and $\lambda \approx 100\,\mathrm{nm}$ is the London penetration depth for an aluminum film of $\sim$50-nm thickness [3]. We obtain $\lambda_J \approx 28\,\mu\mathrm{m}$, approximately one order of magnitude larger than our junction width, justifying the assumption of the linear phase gradient in the junction for finite magnetic fields.

Supplementary Note 4   Surface state coherence length

The Fu-Kane theory [4] assumed that the Josephson junction is in the short-junction limit. This requires the superconducting coherence length ξ_{TI} in the TI surface state to be larger than the junction length $L = 50\,\mathrm{nm}$. The effective coherence length in a non-ballistic junction can be calculated via $\xi_{\mathrm{TI}} = \sqrt{\frac{\hbar v_F l_e}{2\Delta}}$, with l_e the mean free path in the TI surface. If we take $l_e \approx 5\,\mathrm{nm}$ and $v_F = 5.5 \times 10^5$ m/s as in the previous work [1], we obtain $\xi_{\mathrm{TI}} \approx 75\,\mathrm{nm}$, which is indeed longer than the junction length.

Supplementary Note 5   Temperature dependence of the spectra
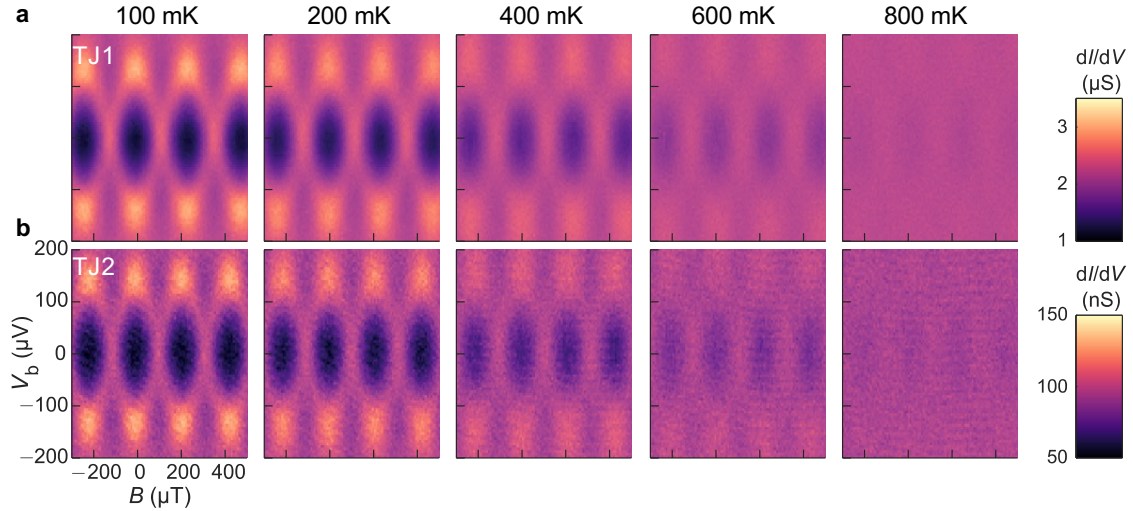

Figure S2: Evolution of the spectra for TJ1 (**a**) and TJ2 (**b**) at $V_G = 0$ with increasing temperature.

In Fig. S2, we show the temperature dependence of the spectra for TJ1 and TJ2 at $V_G = 0$. The gap closing and reopening is essentially robust against increasing temperature, although thermal smearing is evident. Even at $T = 600\,\mathrm{mK}$, the key feature is still recognizable.

3
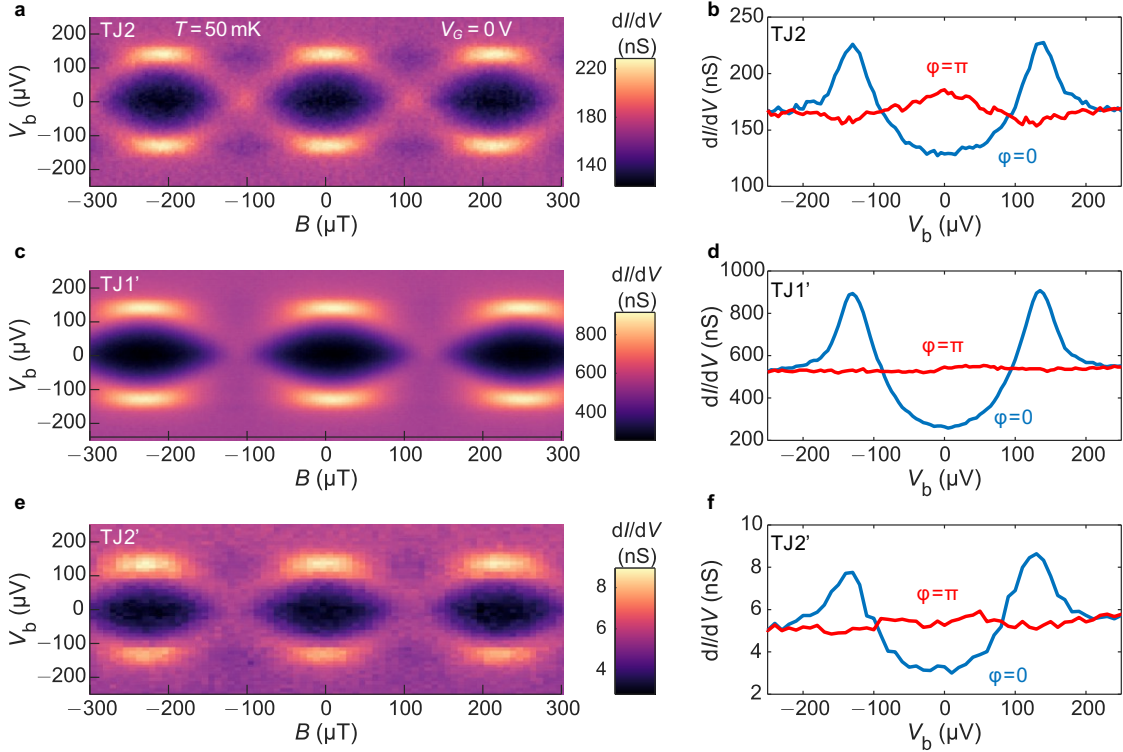
Supplementary Note 6　Confirmation of reproducibility

Figure S3: (a, b) Gap closing and reopening for TJ2 of the device discused in the main text. (c-f) Data on TJ1' and TJ2' made on an identically-designed device fabricted on a different flake of the same crystal. $V_G = 0$ V for all the data. In panels (b), (d), and (f), line cuts at $\varphi = 0$ (blue) and $\varphi = \pi$ (red) are shown for each junction.

In Fig. S3, we show the data for TJ2 at $V_G = 0$ not shown in the main text, as well as the data obtained from a device with an identical design as the one discussed in the main text. It is fabricated on a BiSbTeSe$_2$ flake exfoliated from the same crystal and has tunnel junctions TJ1' and TJ2' in analogous positions. We observe the same closing and reopening of the induced superconducting gap as a function of the phase across the junction as for the device discussed in the main text.

4

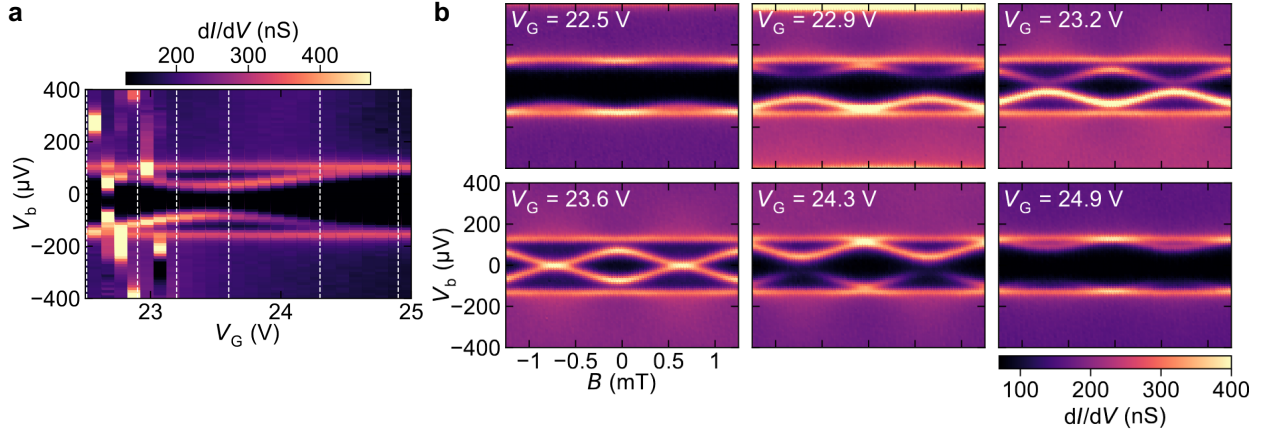## Supplementary Note 7   Observation of spurious resonant states

Figure S4:   **Spurious resonance state.**   **a,** dI/dV spectra as a function of V_G and V_b measured at $\varphi = 0$ in a device similar to the one discussed in the main text. In a narrow V_G range of 22.5 – 25 V, a single ABS appeared in the SC gap. **b,** φ-dependence of the ABS spectra at selected V_G values in this narrow V_G range.

In a device of similar geometry, we observed an induced SC gap, but the spectrum did not change with the phase bias at $V_G = 0$. However, when we swept V_G without applying any phase bias, a sharp and strongly-dispersing Andreev bound state (ABS) appeared in some V_G intervals. An example is shown in Fig. S4a for the V_G-interval of 22.5 – 25 V. The phase-bias dependence of this ABS changes strongly with V_G (Fig. S4b), and interestingly, the state becomes gapless at $V_G =$ 23.6 V where it produced a sharp ZBCP. The electron-hole asymmetry of the ABS switched across $V_G = 23.6$ V. This behavior is consistent with the model for a quantum-dot state in a Josephson junction being tuned in and out of resonance with the superconductor [5]. It is useful to note that this ZBCP appears only at particular V_G values and is not accompanied by low-energy excited states, which is completely different from the gap-closing phenomenology we reported in the main text. As for the origin of this peculiar feature observed in this device, we speculate that due to the uncontrollable nature of our tunnel contacts, the tunnel electrode spuriously did not couple to the

5

TI surface, but rather coupled to a single impurity level in the dielectric with a charging energy that was tuned by V_G.

Supplementary Note 8   Calculation of the Majorana velocity

The Majorana velocity for the Josephson junction in the short-junction limit depends on the length of the junction. Starting from the surface Hamiltonian of the TI and including superconductivity in the Bogoliubov-de Gennes formalism, the full Hamiltonian can be split into

$$H = \underbrace{H_\perp + H_\pi}_{H_{\text{JR}}} + H_\parallel \; ; \tag{S1}$$

$H_\perp$ and $H_\parallel$ denote the momentum component orthogonal and parallel to the junction, respectively, and H_π accounts for the superconductivity for a phase difference of $\varphi = \pi$ across the junction. $H_{\text{JR}} = H_\perp + H_\pi$ is a four-band generalization of the Jackiw-Rebbi model and can be solved exactly for two zero-energy Majorana bound states in the junction. The remaining contributions are included perturbatively and by evaluating $H_\parallel$ to first order we find the Majorana velocity

$$v_M = v_F \frac{\Delta^2}{\Delta^2 + \mu^2} \frac{\cos\left(\frac{\mu L}{\hbar v_F}\right) + \frac{\Delta}{\mu} \sin\left(\frac{\mu L}{\hbar v_F}\right)}{1 + \frac{\Delta L}{\hbar v_F}} \tag{S2}$$

with the TI surface velocity v_F, the magnitude of the superconducting gap Δ, the chemical potential μ, and the length of the junction L. For more information, see Eq. (3.23) of Ref. 6. In the limit $L \ll \hbar v_F / \Delta$, it reduces to the result presented by Fu and Kane in Ref. 4. Moreover, for $\mu \gg \Delta$, we obtain the simple expression $v_M = v_F (\Delta/\mu)^2$ mentioned in Ref. 7. We note that the assumption of a single transversal mode, which lies behind the calculations, is valid for $\mu < \hbar v_F / L$.

Supplementary Note 9   Simulation of the TI Josephson junction

To qualitatively determine the differential conductance of the TI Josephson junction, a transport simulation for a three-dimensional tight-binding experiment was performed using the Python library Kwant. As a model for the three-dimensional strong topological insulator, the Bernevig-Hughes-Zhang (BHZ) model was chosen. In the basis $\mathbf{\Psi} = ((\Psi_\uparrow^1, \Psi_\downarrow^1), (\Psi_\uparrow^2, \Psi_\downarrow^2))^T$, where $i = 1, 2$ is denoting the orbital and $\uparrow, \downarrow$ the spin, the full BHZ Hamiltonian is given by

$$H_{\text{BHZ}} = (\epsilon_0(\boldsymbol{k}) - \mu) + M(\boldsymbol{k})\,\hat{\pi}_z + A_1\,k_z\,\hat{\pi}_x\hat{\sigma}_z + A_2(k_x\hat{\pi}_x\hat{\sigma}_x + k_y\,\hat{\pi}_x\hat{\sigma}_y) \tag{S3}$$

with

$$\epsilon_0(\boldsymbol{k}) = C + D_1 k_z^2 + D_2(k_x^2 + k_y^2) \quad \text{and} \tag{S4}$$

$$M(\boldsymbol{k}) = M - B_1 k_z^2 - B_2(k_x^2 + k_y^2)\,. \tag{S5}$$

The Pauli operators $\hat{\boldsymbol{\pi}}$ act on the orbital degree of freedom and $\hat{\boldsymbol{\sigma}}$ on the spin degree of freedom. In our notation, tensor products of different Pauli operators are always implied, and identity operators acting are not written explicitly. For our purposes we use the simplest version of the model in Eq. (S3) that exhibits a topological phase. We neglect the spin and orbital independent part of the spectrum $\epsilon_0(\boldsymbol{k})$ by setting $C = D_j = 0$ and choose

$$A_1 = A_2 = v \quad \text{and} \quad B_1 = B_2 = \frac{v}{2|M|}\,. \tag{S6}$$

With this choice of parameters, the Hamiltonian simplifies to

$$H_{\text{BHZ}} = -\mu + (M - \frac{v}{2|M|}\,\boldsymbol{k}^2)\hat{\pi}_z + v\hat{\pi}_x\,\boldsymbol{k}\cdot\hat{\boldsymbol{\sigma}}\,. \tag{S7}$$

7

The model exhibits a topological gap $2|M|$ and a Dirac surface spectrum with the Dirac velocity v, which is set to 1 in the simulation. Furthermore, the parameter M was set to 1. The reduced model is implemented as a tight-binding model on a cubic lattice in Kwant. The full simulation of the bulk of the TI is necessary to obtain correct surface states. For the inclusion of superconductivity in the system, the time reversed states of the BHZ model were implemented as additional orbitals to explicitly simulate a Bogoliubov–de-Gennes (BdG) Hamiltonian. On the surface of the TI, a finite superconduction gap $\Delta = 0.1e^{i\varphi}$ is opened by coupling the two sectors of the BdG-Hamiltonian. Two superconducting regions are separated by a bare TI surface of fixed width on the top of the sample, thus modeling a Josephson junction of the surfaces by varying φ across the junction. Only on that strip of bare TI surface the gapless surface state are found. On all other surfaces, the surface states are gapped away by the finite superconductivity. The phase variation created by the magnetic field in the experiment is implemented directly. On the bottom surface, the phase jump is split up into two steps to prevent hybridisation between the surface state in the TI JJ and unphysical Andreev bound state on the lower surface of the sample. The cross section geometry is sketched in Fig. S5. The dimensions of the simulation in units of the lattice constant are $W = 9$, $W_{\text{SC}} = 8$, $W'_{\text{SC}} = 1$, $W_T = 9$, $D = 12$ and $D_{\text{SC}} = 1$. The system is extended infinitely along the junction and probed by a tunnel lead attached vertically to the bare TI region at one point. The tunnel lead is simulated as a normal conducting cubic lattice and the tunnel contact is tuned by varying the hopping from the lead into the system. The differential conductivity is calculated as a function of the energy E compared to the superconducting gap Δ and the phase difference across the Josephson junction ϕ_B.
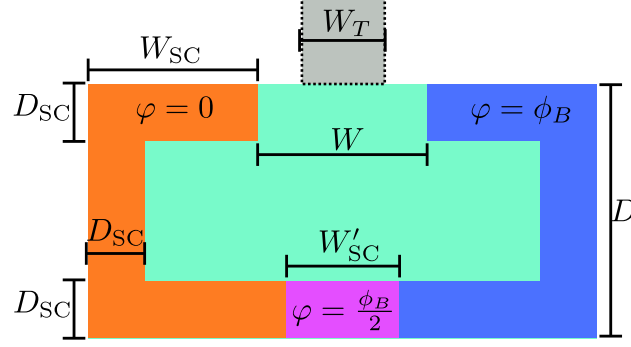
Figure S5: **Sketch of the simulated system.** The cross section of the simulated system shown with its dimensions. The bulk TI in the center (turquoise) is surrounded by three separate regions with finite superconducting gap Δ (orange, purple, blue). The phase of the gap function φ differs between the regions. On the top surface, this creates a Josephson junction with a finite width W and the phase difference ϕ_B. A tunnel lead (gray) is attached in the center of the bare TI surface of the junction.

References

1. Ghatak, S. <u>et al.</u> Anomalous Fraunhofer patterns in gated Josephson junctions based on the bulk-insulating topological insulator BiSbTeSe$_2$. <u>Nano Lett.</u> **18**, 5124–5131 (2018).

2. Zhang, W., Yu, R., Zhang, H.-J., Dai, X. & Fang, Z. First-principles studies of the three-dimensional strong topological insulators Bi$_2$Te$_3$, Bi$_2$Se$_3$ and Sb$_2$Te$_3$. <u>New J. Phys.</u> **12**, 065013 (2010).

3. López-Núñez, D. <u>et al.</u> Magnetic penetration depth of aluminum thin films. <u>arXiv:2311.14119</u> (2023).

4. Fu, L. & Kane, C. L. Superconducting proximity effect and Majorana fermions at the surface of a topological insulator. <u>Phys. Rev. Lett.</u> **100**, 096407 (2008).

5. Oriekhov, D. O., Cheipesh, Y. & Beenakker, C. W. J. Voltage staircase in a current-biased quantum-dot Josephson junction. <u>Phys. Rev. B</u> **103**, 094518 (2021).

6. Montag, A.   Master's thesis, RWTH Aachen University (2023).   Available   at `https://www.quantuminfo.physik.rwth-aachen.de/global/show_document.asp?id=aaaaaaaacerwruu`.

7. Potter, A. C. & Fu, L. Anomalous supercurrent from Majorana states in topological insulator josephson junctions. <u>Phys. Rev. B</u> **88**, 121109 (2013).